AN INTERLEAVED ISOLATED THREE-PHASE SEPIC DC-DC CONVERTER WITH COUPLED INPUT INDUCTORS

FERNANDA R. PAULO, ROMERO L. ANDERSEN

Department of Electrical Engineering, Federal University of Paraíba
Caixa Postal 5115, Campus I - Cidade Universitária CEP: 58059-970, João Pessoa - PB, Brasil
E-mails: fernanda.paulo@cear.ufpb.br, romero@cear.ufpb.br

Abstract— This paper presents the analysis of a three-phase interleaved SEPIC DC-DC converter with coupled input inductors and isolated by three single phase transformers. The number of magnetic components is reduced when coupled inductors are used in the input. Besides that, a reduced current ripple is achieved. A detailed theoretical analysis is presented describing the operation stages for a duty cycle from 2/3 to 1, in both continuous and discontinuous conduction mode. The effect of the coupling factor in the input current ripple and in the operation of the converter was also evaluated. A design example is presented for a 500 W converter with 80 V input voltage, 400 V output voltage and 40 kHz switching frequency. To validate the analysis, some experimental results are also presented.

Keywords— SEPIC converter, interleaved converters, DC-DC power conversion, coupled inductors, three-phase DC-DC converters.

Resumo— Nesse trabalho é apresentada a análise de um conversor CC-CC SEPIC *interleaved* trifásico com indutores de entrada acoplados e isolado por três transformadores monofásicos. O número de elementos magnéticos é reduzido usando os indutores de entrada acoplados. Além disso, também é reduzida a ondulação da corrente de entrada. Uma análise teórica detalhada é apresentada descrevendo as etapas de operação para uma razão cíclica entre 2/3 e 1, tanto para o modo de condução contínua quanto descontínua. O efeito do fator de acoplamento na ondulação de corrente de entrada e na operação do conversor é avaliado. Um exemplo de projeto é apresentado para um conversor de 500 W com uma tensão de entrada de 80 V, uma tensão de saída de 400 V e uma frequência de chaveamento de 40 kHz. Para validar a análise, alguns resultados experimentais também são apresentados.

Palavras-chave— Conversor SEPIC, conversores intercalados, conversão de energia CC-CC, indutores acoplados, conversores CC-CC trifásicos.

1 Introduction

The demand for electricity has been increasing and the interest in alternative sources became evident in a global scenario of limited non-renewable energy sources and attention to sustainability. In recent years, researches on technologies that involve the usage of photovoltaic (PV) panels and wind turbines are noteworthy. However, the output characteristic of these power sources is generally not appropriate to fed most of loads directly and DC-DC converters are necessary (Moradpour et al., 2018).

The low output voltage of PV panels, for example, must be step-up to be appropriate for grid integration (Moradpour et al., 2018) and in order to perform a maximum power point tracking the converter should have a continuous input current (Moradpour et al., 2018). These systems have also an intermittent nature and supplemental power sources are required (Haghighian et al., 2017), as batteries, and the converter must be able to operate within the variations and supply constant voltage over the battery range (Kircioglu et al., 2016).

The single-ended primary inductor converter (SEPIC) has been used in renewable sources applications, as in Moradpour et al. (2018) and Gules et al. (2014), due to its step-down or step-up operation, noninverted output voltage and low input current ripple (Lee & Do, 2018). The SEPIC was originally proposed as an alternative to the conventional push-pull converter, which inherently had a voltage source characteristic (Massey & Snyder,1977).

In general, to reduce current ripple a large inductor can be used. However, this approach increases the size of the converter. Other methods adopted are the usage of coupled inductors (Do, 2012)(Lee & Do, 2017) and interleaved converters (Shi et al., 2016). The interleaving technique is also used to make the converter more suitable for higher power applications.

Three-phase interleaved topologies have been studied as a way to improve the converter power density and efficiency (Kattel et al., 2016)(Rahimi et al., 2017). In these structures, each phase of the converter works in its own period, out phased from the others, with the same duty cycle and rms current (Rahimi et al., 2017). As the need for higher power levels increased, the three-phase systems were acquiring notoriety. The advantages of three-phase converters over the single-phase counterpart include lower component stresses and reduced input and output filter requirements (Kattel et al., 2016)(Agostini & Barbi, 2011).

In (Shi et al., 2016), a two-phase SEPIC interleaved was proposed. The converter was design with coupled inductors in order to reduce the number of magnetic cores and the current ripple in the discontinuous conduction mode (DCM) operation.

In this paper, in order to include the advantages of three-phase systems to the SEPIC converter, and reduce the number of magnetic components, a three-phase interleaved SEPIC with coupled inductors in the input is presented.

The effect of the coupling factor of the input inductors in the current ripple and in the operation mode is evaluated. In this topology, the load is isolated from the source through single-phase transformers in each of the three phases. The transformers are connected in wye in both sides, and the central point of the primary side is connected to the negative terminal of the power source.

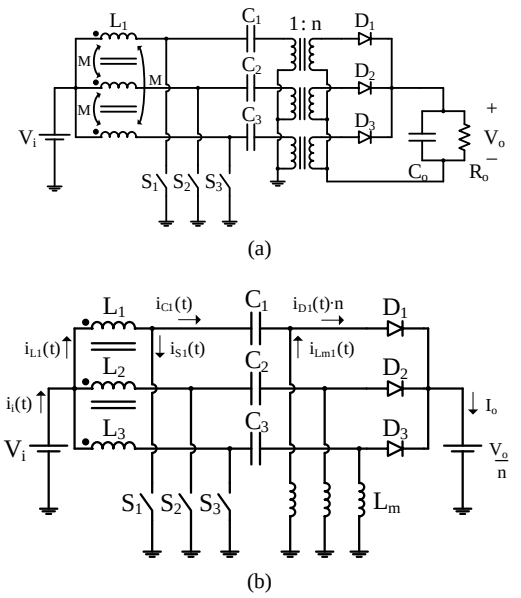

Figure 1. Circuit of the three-phase interleaved dc-dc converter SEPIC with coupled inductors. (a) Proposed configuration. (b) Non-isolated version.

2 Proposed Converter

The circuit of the interleaved three-phase SEPIC DC-DC converter with coupled inductors is shown in Figure 1(a). The proposed converter operates in three different regions according to the duty cycle, D: R1, in which $0 < D < 1/3$; R2, in which $1/3 < D < 2/3$; and R3, in which $2/3 < D < 1$. In this paper, the region R3 was chosen to illustrate the principle of operation. In this region, up to three switches are simultaneously on.

To simplify the analysis of the converter, the non-isolated version of the circuit, shown in Figure 1(b), was considered. The following assumptions are made: the capacitances are dimensioned such that, in steady state, the voltage ripple is negligible; the self-inductances are identical and $L_1 = L_2 = L_3 = L$; the mutual inductances and coupling coefficients are equal to all three phases; switches and diodes are ideal; n is the turns ratio N_2/N_1.

2.1 CCM Operation Analysis

In continuous conduction mode (CCM) operation of region R3, the proposed converter has six stages per switching period. Figure 2 shows the different stages. Before the first stage, S_2 and S_3 are already conducting.

1) First stage (t_0, t_1): all switches are on and all the diodes are off, as shown in Figure 2(a). The voltage across L of all phases is V_i and the current $i_L(t)$ increase linearly.

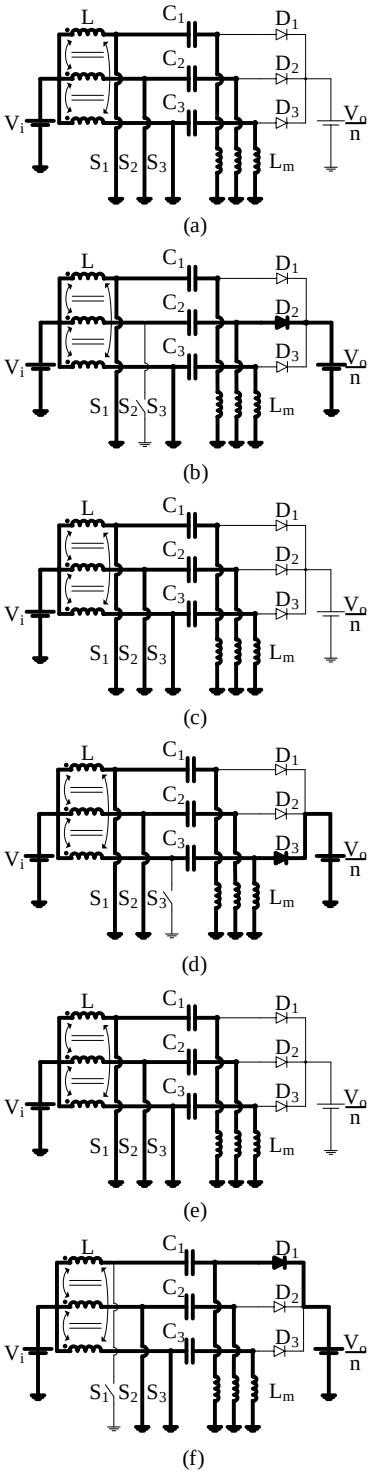

Figure 2. Topological stages of CCM Operation in Region R3. (a) First stage. (b) Second stage. (c) Third stage. (d) Fourth stage. (e) Fifth stage. (f) Sixth stage.

2) Second stage (t_1, t_2): the switch S_2 is turned off and the load receives energy through the diode D_2, as shown in Figure 2(b). The current $i_{L2}(t)$ is now decreasing linearly.

The third and fifth stages are similar to the first stage; the fourth and sixth stages are similar to the second stage; the difference is the switches that are on. After sixth stage, the switching period is complete. The main theoretical waveforms of the CCM operation in region R3 are shown in Figure 3. Phase 1 was considered, however phases 2 and 3 are identical only shifted by 120º.

To perform the mathematical analysis of the converter, it is considered that the coupled inductors structure consists in three windings wound on the central leg. The voltage across one winding can be expressed as a result of its total flux linkage due to all the windings on the core. Considering the selves and mutual inductances to be the same, the terminal voltage of the windings can be expressed as (1).

$$\begin{bmatrix} v_{L1}(t) \\ v_{L2}(t) \\ v_{L3}(t) \end{bmatrix} = \begin{bmatrix} L & M & M \\ M & L & M \\ M & M & L \end{bmatrix} \frac{d}{dt} \begin{bmatrix} i_{L1}(t) \\ i_{L2}(t) \\ i_{L3}(t) \end{bmatrix} \quad (1)$$

Where M = k·L, considering the coupled inductors structure. The coupling factor, or coupling coefficient, k is a measure of the degree of magnetic coupling between two windings (Erickson & Maksimovic, 2001).

In CCM operation, the average voltage through one inductor coil, as represented in equation (2), determines the voltage gain. The waveform of the voltage can be seen in Figure (3).

$$V_L = \frac{1}{T_S} \cdot \left[\int_0^{D \cdot T_S} V_i dt + \int_0^{(1-D) \cdot T_S} -\frac{V_o}{n} dt \right] = 0 \quad (2)$$

Equation (3) leads to the input-output voltage gain.

$$q = \frac{V_o}{V_i} = n \cdot \frac{D}{(1-D)} \quad (3)$$

To calculate the variation of the inductor's current corresponding to each stage, the voltage across L and the time interval are verified and substituted in equation (1). In the first stage, the voltage across L is V_i in all phases. In the second stage, the voltage across L is V_i in the phases with the switch on and $-V_o/n$ in the phase with the switch off. The expressions for the time intervals of Figure 3 can be seen in Table 1. The results to the first and second stages after isolating the variations are expressed in equation (4) and (5) respectively.

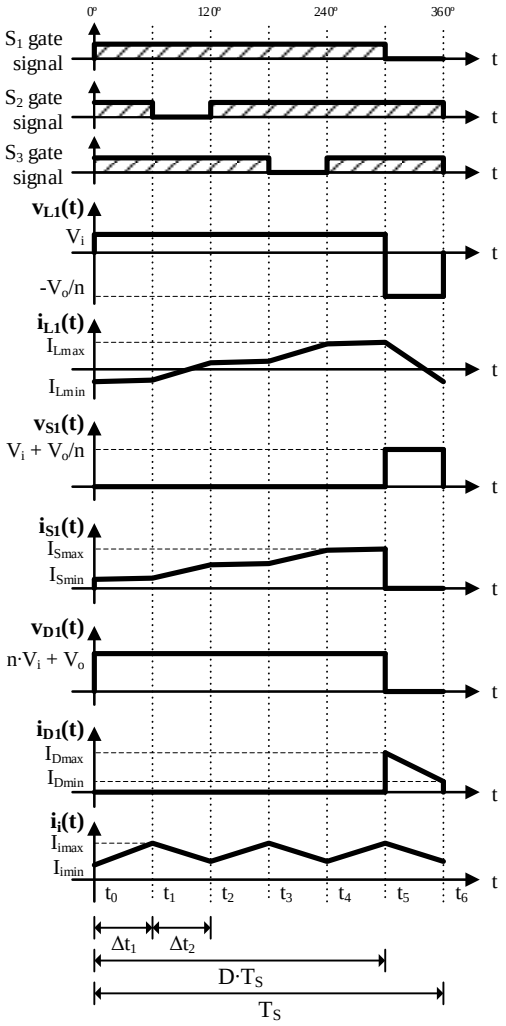

Figure 3. Main theoretical waveforms for CCM in region R3.

$$\Delta I_{Lon} = \frac{V_i \cdot (3D-2)}{3 \cdot L \cdot f \cdot (2k+1)} \quad (4)$$

Table 1. Equations for time intervals of Figure 3.

Stage	Equation
First stage	$\Delta t_1 = \left(D - \frac{2}{3}\right) \cdot T_s$
Second stage	$\Delta t_2 = (1-D) \cdot T_s$

$$\Delta I_{Lon} = \frac{(V_o \cdot k + V_i \cdot n) \cdot (1-D)}{L \cdot n \cdot f \cdot (-2k^2 + k + 1)}$$
$$\Delta I_{Loff} = \frac{(2 \cdot V_i \cdot k \cdot n + V_o + V_o \cdot k) \cdot (1-D)}{L \cdot n \cdot f \cdot (-2k^2 + k + 1)} \quad (5)$$

The input current ripple is the sum of the three inductors current ripples in the first or second stage. Considering the first stage, equation (6) is obtained.

$$\Delta I_i = \frac{V_i \cdot (3D-2)}{L \cdot f \cdot (2k+1)} \quad (6)$$

2.2 DCM Operation Analysis

In DCM operation, the proposed converter has nine stages per switching period, as shown in Figure 4. The first and second stage are similar to CCM operation. Before the third stage, S_1 and S_3 are conducting.

3) Third stage (t_2, t_3): the current across the diode D_2 is zero and all the diodes are off. Considering an equivalent inductance between the magnetizing inductance of the transformer and the self-inductance L of the phase 2, there is no electric potential difference and the current in these elements maintains constant. Since the voltage across them are equal and of opposite polarity, it can assume any value. Due to the coupling of the magnetic core, this voltage will be $2 \cdot k \cdot V_i/(1+k)$.

The fourth and seventh stages are similar to the first stage; the fifth and eighth stages are similar to the second stage; the sixth and ninth stages are similar to the third stage. The main theoretical waveforms of the DCM operation are shown in Figure 5.

As in the CCM operation, to calculate the variation of the inductor's current, the voltage across an inductor winding and the time interval must be observed and substituted in equation (1). For the first stage, the ripple will be the same as equation (4). For the second stage, only the expression of the time interval will change.

Therefore, it is possible to find the current variations in the second stage through equation (1) as shown in equation (7).

$$\Delta I_{Lon} = \frac{(V_o \cdot k + V_i \cdot n)}{L \cdot n \cdot (-2k^2 + k + 1)} \cdot \Delta t_2$$
$$\Delta I_{Loff} = \frac{(2 \cdot V_i \cdot k \cdot n + V_o + V_o \cdot k)}{L \cdot n \cdot (-2k^2 + k + 1)} \cdot \Delta t_2 \quad (7)$$

In regard to the equation (8) the variation of the inductor's current can be determined to the interval $\Delta t_3 = (1 - D) \cdot T_S - \Delta t_2$, when the voltage across L is V_i through the phases with the switch on and $2 \cdot k \cdot V_i/(1+k)$ through the phase with no current variation.

$$\Delta I_{Lon} = \frac{V_i}{L \cdot (k + 1)} \cdot \Delta t_3 \quad (8)$$

The time interval Δt_2 can be obtained from the average current across one diode. Observing Figure 5 equation (9) can be expressed, where ΔI_{Loff} is the variation of the inductor's current when $\Delta t = \Delta t_2$.

$$n \cdot I_{Dmed} = \frac{1}{T} \cdot \frac{\Delta I_{Loff} \cdot \Delta t_2}{2} \quad (9)$$

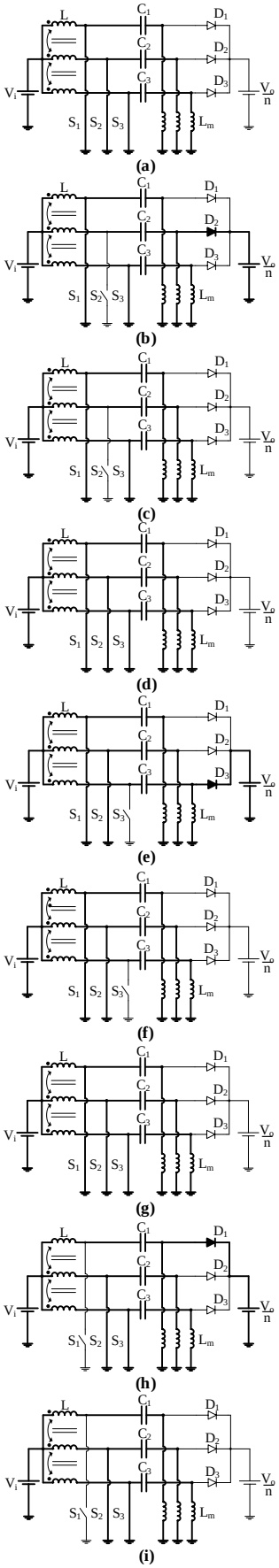

Figure 4. Topological stages of DCM Operation in Region R3. (a) First stage. (b) Second stage. (c) Third stage. (d) Fourth stage. (e) Fifth stage. (f) Sixth stage (g) Seventh stage (h) Eighth stage. (i) Ninth Stage.

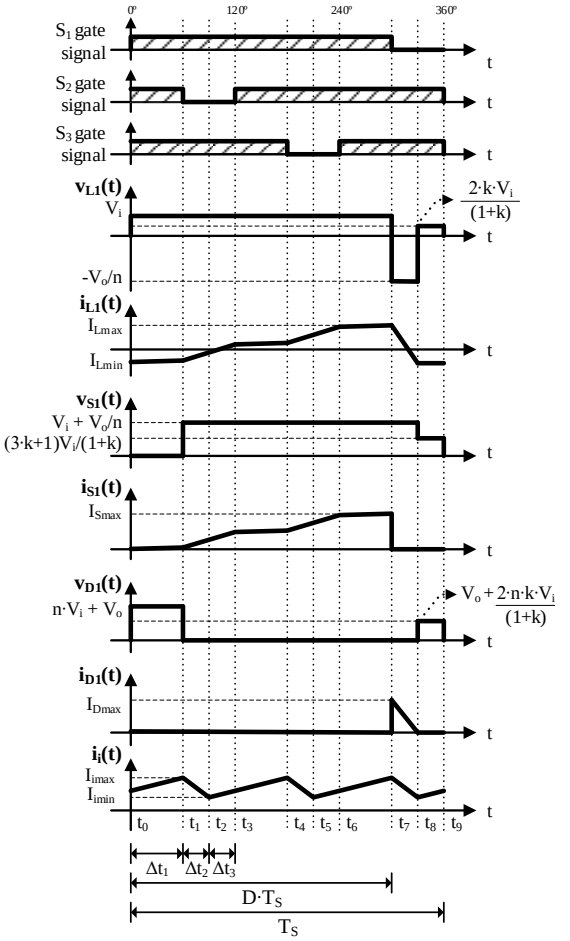

Figure 5. Main waveforms for DCM in region R3.

Equation (9) leads to the time interval Δt_2 presented in equation (10) when (7) is considered and knowing that $I_{Dmed} = I_o/3 = V_o/(3 \cdot R_o)$ as expected from the circuit analysis.

$$\Delta t_2 = \sqrt{\frac{2 \cdot n \cdot V_o \cdot L \cdot n \cdot (-2k^2 + k + 1)}{3 \cdot R_o \cdot f \cdot (2 \cdot V_i \cdot k \cdot n + V_o + V_o \cdot k)}} \qquad (10)$$

The average voltage through one inductor coil determines the voltage gain, which is zero in steady state. It can be written as (11).

$$V_L = \frac{1}{T} \cdot \left[V_i \cdot (3 \cdot \Delta t_1 + 2 \cdot \Delta t_2 + 2 \cdot \Delta t_3) - \frac{V_o}{n} \cdot \Delta t_2 + \frac{2 \cdot k \cdot V_i}{(k+1)} \cdot \Delta t_3 \right] \qquad (11)$$

Equation (12) leads to the voltage gain. An iterative calculation of these equations is suggested to determine simultaneously the gain and the time intervals.

$$q = \frac{n \cdot [(3 \cdot \Delta t_1 + 2 \cdot \Delta t_2 + 2 \cdot \Delta t_3) \cdot (k+1) + 2 \cdot k \cdot \Delta t_3]}{\Delta t_2 \cdot (k+1)} \qquad (12)$$

The input current ripple is the sum of the three inductors current ripples in the time interval consisting of Δt_2 or $\Delta t_3 + \Delta t_1$ as can be seen in Figure 5. Considering the former, equation (13) is obtained.

$$\Delta I_i = \frac{(2 \cdot V_i \cdot k \cdot n - 2 \cdot V_i \cdot n + V_o - V_o \cdot k) \cdot \Delta t_2}{L \cdot n \cdot (-2k^2 + k + 1)} \qquad (13)$$

2.3 Boundary between Continuous and Discontinuous Conduction Modes

In the limit between CCM and DCM, the static gains of both cases are equivalent and only two time intervals exist, Δt_1 and Δt_2, as in Table 1.

Considering equation (10) of Δt_2 and substituting the gain in (3) and the expressions in Table 1, when isolating the value of R_o it is possible to define a $R_{critical}$ as in (14). $R_{critical}$ refers to the limit between CCM and DCM when $R_o = R_{critical}$. If $R_o < R_{critical}$, the CCM is achieved.

$$R_{critical} = \frac{2 \cdot D \cdot L \cdot f \cdot n^2 \cdot (-2k^2 + k + 1)}{3 \cdot (D-1)^2 \cdot (D + 2 \cdot k - D \cdot k)} \qquad (14)$$

Another possibility is to delimit the discontinuity from $k_{critical}$ when isolating the value of k from equation (14) and substituting $R_{critical}$ by R_o. If $k < k_{critical}$, the CCM is achieved.

3 Design Example

In order to simulate the converter and implement a prototype, design specifications were defined as follows: P_o = 500 W, V_i = 80 V, V_o = 400 V, f_s = 40 kHz and $\Delta I_i = 0.95\% I_i = 0.0594$ A. The duty cycle was chosen 0.8 to assure the operation in region R3. The CCM was chosen because of its simpler expressions.

The turns ratio was calculated from the voltage gain equation of the CCM operation presented in (3) as can be seen in (15).

$$n = \frac{V_o}{V_i} \cdot \frac{(1-D)}{D} = \frac{400}{80} \cdot \frac{(1-0{,}8)}{0{,}8} = 1.25 \qquad (15)$$

The input current ripple of CCM can be calculated through equation (6) and it is inversely proportional to self-inductance L and the coupling factor k. Thus, there are multiple combinations to the desired ripple current.

One way to acquire these parameters is to determine how far one wants to work from the discontinuity limit. As seen in section 2.3, if k is greater than $k_{critical}$, the conduction mode becomes discontinuous and ΔI_i will be as equation (13). Unlike the CCM, the current ripple in the DCM depends on the value of V_o which increases with the entrance in deep DCM and

hence makes it difficult to maintain a low current ripple. This situation is illustrated in Figure 6. With the value of n = 1.25, a limit to k was chosen as 90% of $k_{critical}$.

In this way, it is possible to iterate equations (6) and (14) to determine L and k. First L is determined by (6) with k = 90% $k_{critical}$, randomly initialized. Then, a new $k_{critical}$ is calculated in function of L through (14) where R_o will substitute $R_{critical}$ and k will be isolated. Then $k_{critical}$ will be compared to the first considered value of k and if it is equal to the stipulated limit, then L and k was determined. If not, iterate again with k equal to the limit. A flowchart is shown in Figure 7 with the calculation sequence.

With ΔI_i = 0.95%I_i, the results can be seen in Table 3.

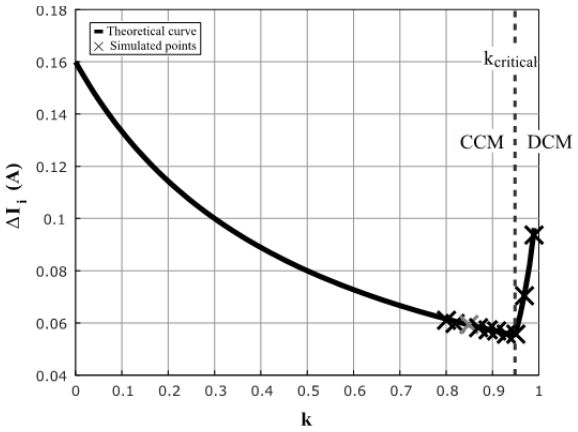

Figure 6. Input current ripple in function of k (V_i = 80 V, fs = 40 kHz, L = 5 mH, R_o = 320 Ω). The grey mark is the operating point.

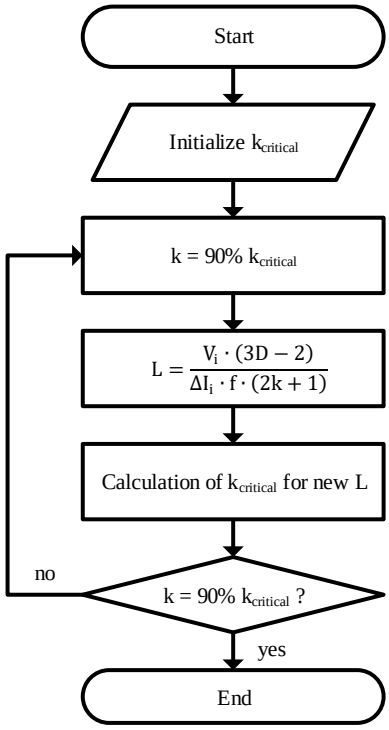

Figure 7. Steps to determinate L and k to a requested ripple current.

5 Experimental Results

After validating the theoretical analysis of the converter through simulations, a prototype was implemented and can be seen in Figure 9. The specifications were chosen with the same parameters of the design example and the components are shown in Table 4. The inductor was constructed, Figure 10, and the coils were wound one below the other. The measurements involving this inductor are presented in Table 5.

The experiments were tested for a nominal output voltage of 400 V. Although the prototype was designed for 500 W, additional unexpected losses were observed in laboratory and for that reason the maximum processed power tested was 300 W. The output voltage and the input current are shown in Figure 11 and Figure 12, respectively. A mean current of 5.5 A and a ripple of 320 mA was obtained.

Table 3. Values obtained for L and k.

Parameter	Value
L	5 mH
k	0,85
$k_{critical}$	0,94

Table 4. Components of the prototype.

Description	Values
Transformers	N_1/N_2 = 0.8
Primary capacitors	10 μF/200 V polypropylene
Output capacitor	470 μF/450 V electrolytic
MOSFETs	SPW17N80C3
Diodes	IDH02G120C5
Digital Signal Controller	dsPIC33EP512MU810

Table 5. Values measured in the coupled inductor.

L	Value	k	Value
L_{11}	4.813 mH	k_{12}	0.936
L_{22}	4.954 mH	k_{23}	0.938
L_{33}	5.073 mH	k_{31}	0.860

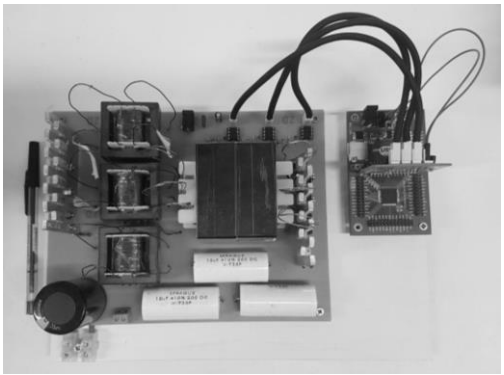

Figure 9. Picture of the prototype.

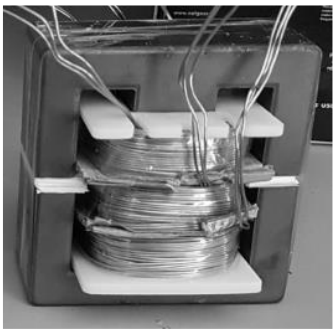

Figure 10. Constructed inductor.

The waveforms of the currents in the coupled inductors can be seen in Figure 12. Although the waveforms are different from Figure 3 and an imbalance is noted in those currents with one phase processing more power than the other. When the values from Table 5 are considered in simulation, the currents in the inductor behave as in Figure 13. This result is presented to 500 W, demonstrating that even then the result is very similar to the waveforms obtained. With a more balanced inductor, the currents would tend to resemble more the theoretical analysis.

The voltages across the switches are shown in Figure 14. Due to the leakage inductances present in the circuit, an overvoltage can be seen, however the peak voltages are below the component limit.

In addition to the waveforms the converter efficiency was analyzed as a function of the output power. The measured values for the various powers are shown in Figure 15. After reaching 200 W output, the converter efficiency started to decrease and was in values lower than theoretically expected. One possible cause would be an effect on the coupled inductors' coils called the proximity effect: given the proximity between conductors carrying alternating currents, the current distribution in these conductors will be altered and restricted to smaller regions. This effect causes an increase in resistance, resulting in losses by Joule effect, and is aggravated by increasing frequency.

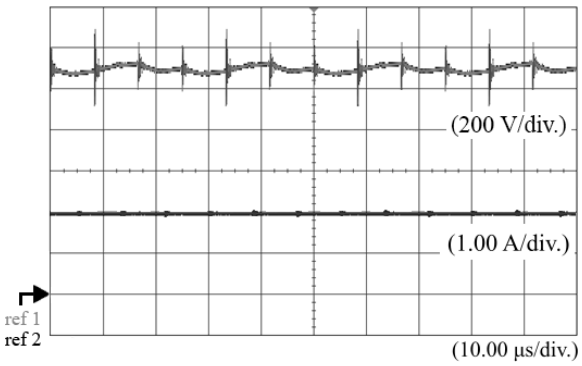

Figure 11. Input current I_i and output voltage V_o.

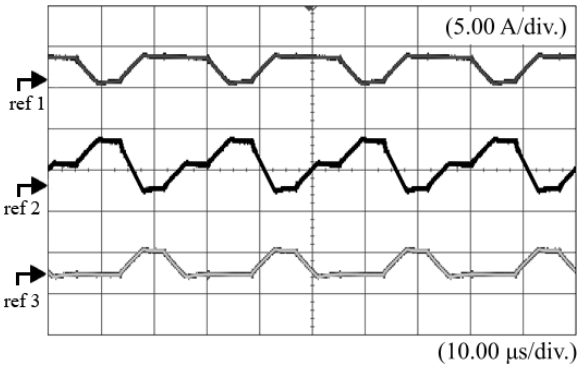

Figure 12. Currents through the inductor i_{L1}, i_{L2}, i_{L3}.

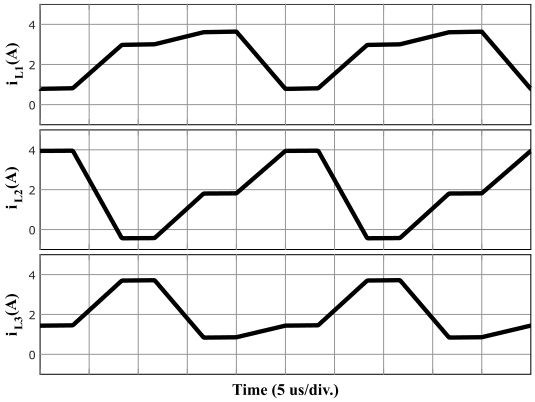

Figure 13. Simulated currents through the inductor i_{L1}, i_{L2}, i_{L3}.

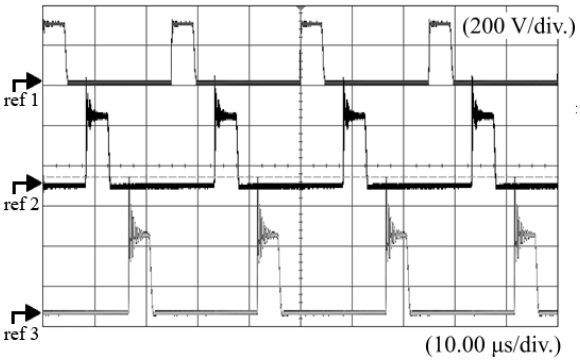

Figure 14. Voltages across the switches v_{S1}, v_{S2}, v_{S3}

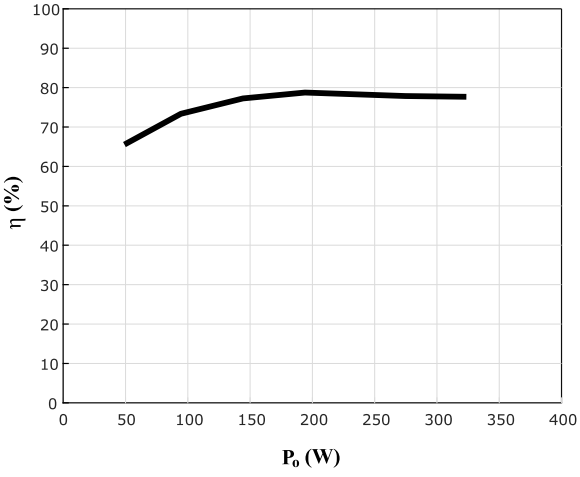

Figure 15. Converter efficiency η as a function of P_o.

6 Conclusions

In this paper, a three-phase interleaved SEPIC with coupled inductors was proposed. A theoretical analysis was presented with the description of the operation stages, specifically for region R3, and the main theoretical waveforms were discussed. Equations were developed, including the input current ripple and the limit between CCM and DCM operation as a function of the coupling factor.

In addition to influencing the conduction mode, the coupling factor also influenced the DCM static gain and the current ripple. Due to this, it was possible to obtain very low current ripples, especially when compared to the original SEPIC, or even a three-phase interleaved SEPIC without coupled inductors.

The operation of the converter was verified by the implementation of a prototype. The waveforms were obtained in which one can observe the coherence between theory and application, in spite of the presence of unbalanced phases due to the structure of the coupled inductor. High losses were also noticed in the converter compared to what was expected in theory, probably due to the inductor.

Future work may involve studies of new ways to construct the coupled inductor, seeking balanced values of k and the reduction of the converter's losses. In addition, dynamic modeling and control of the converter can also be done.

References

Agostini Jr., E. and Barbi, I. (2011). Three-Phase Three-Level PWM DC–DC Converter. IEEE Transactions on Power Electronics, vol. 26, no. 7, pp. 1847-1856.

Do, H. (2011). Soft-Switching SEPIC Converter With Ripple-Free Input Current. IEEE Transactions on Power Electronics, vol. 27, no. 6, pp. 2879-2887.

El Kattel, M. B.; Mayer, R. and Oliveira, S. V. G. (2016). Analysis and simulation of a three-phase push-pull/flyback interleaved bidirectional dc-dc converter. In: IECON 2016 - 42nd Annual Conference of the IEEE Industrial Electronics Society. Florence: IEEE, pp. 1274-1279.

Erickson, R. W. and Maksimovic, D. (2001). Fundamentals of Power Electronics. New York: Kluwer Academic/Plenum Publishers.

Gules, R.; Santos, W. M.; Reis, F. A.; Romaneli, E. F. R.; Badin A. A. (2014). A Modified SEPIC Converter With High Static Gain for Renewable Applications. IEEE Transactions on Power Electronics, vol. 29, no. 11, pp. 5860-5871.

Haghighian, S. K.; Tohidi, S.; Feyzi, M. R. and Sabahi, M. (2017). Design and analysis of a novel SEPIC-based multi-input DC/DC converter. IET Power Electronics, vol. 26, no. 3, pp. 923-930.

Kircioglus, O.; Ünlü, M. and Çamur, S. (2016). Modeling and Analysis of DC-DC SEPIC Converter with Coupled Inductors. In: International Symposium on Industrial Electronics. Banja Luka: IEEE, pp. 1-5.

Lee, S. and Do, H. (2018). Isolated SEPIC DC–DC Converter With Ripple-Free Input Current and Lossless Snubber. IEEE Transactions on Industrial Electronics, vol. 65, no. 2, pp. 1254-1262.

Lee, S. and Do, H. (2017). Zero-Ripple Input-Current High-Step-Up Boost–SEPIC DC–DC Converter With Reduced Switch-Voltage Stress. IEEE Transactions on Power Electronics, vol. 32, no. 8, pp. 6170-6177.

Massey, R. P. and Snyder, E. C. (1977). High voltage single-ended DC-DC converter. In: 1977 IEEE Power Electronics Specialists Conference. Palo Alto, CA, USA: IEEE, pp. 156-159.

Moradpour, R.; Ardi, H. and Tavakoli, A. (2018). Design and Implementation of a New SEPIC-Based High Step-Up DC/DC Converter for Renewable Energy Applications. IEEE Transactions on Industrial Electronics, vol. 65, no. 2, pp. 1290-1297.

Rahimi, T.; Hosseini, S. H.; Sabahi, M.; Abapour, M. and Gharehpetian, G. B. (2017). Three-phase soft-switching-based interleaved boost converter with high reliability. IET Power Electronics, vol. 10, no. 3, pp. 377-386.

Shi, C.; Khaligh, A. and Wang, H. (2016). Interleaved SEPIC Power Factor Preregulator Using Coupled Inductors In Discontinuous Conduction Mode With Wide Output Voltage. IEEE Transactions on Industry Applications, vol. 52, no. 4, pp. 3461-3471.